5. MHD EQUILIBRIUM AND STABILITY

This chapter deals with the MHD equilibrium and stability properties of the reference QPS configuration: vacuum and finite-beta flux surfaces, possible existence of magnetic islands or ergodic regions, bootstrap current alignment, ideal MHD stability of Mercier, ballooning, kink, and vertical modes, and finally, a brief discussion of resistive MHD stability.

5.1. Introduction

The MHD equilibrium and stability of the reference configuration are discussed in this chapter. An important issue at the very low aspect ratio (A ~ 2.5) of QPS is the existence of vacuum magnetic flux surfaces. The existence of magnetic islands or ergodic regions (both effectively increase the actual aspect ratio) will be addressed, along with a discussion of the sensitivity of vacuum flux surfaces to different coil currents. This is followed by a comparison of the MHD equilibrium at finite β between the fixed and free-boundary calculations. The QPS experiment has been designed to run with both Ohmic current (particularly at low β) as well as a current profile fully compatible ("aligned") with the bootstrap current. The issue of bootstrap *alignment* and *consistency* (i.e., where the bootstrap current is computed self-consistently from the ι and p profiles, and the |B| spectra) for the reference configuration will be discussed.

This chapter also examines ideal MHD stability of Mercier, ballooning, kink, and vertical modes for the reference configuration. Finally, the resistive MHD stability in QPS will be discussed briefly.

5.2. Properties of Vacuum Configuration

Figure 5.1 shows a Poincaré plot of the vacuum flux surfaces obtained from following magnetic field lines for the reference set of QPS coils using the AVAC code[1]. The outer black curve in these figures is the last closed flux surfaces (LCFS) as obtained from the free-boundary VMEC code for the same set of coils. A variety of ι profiles, corresponding to different amounts and sign of shear, are found to be accessible by appropriately varying the modular, PF and TF coil currents. This gives the QPS experiment the flexibility to investigate flux surface integrity, bootstrap current dependence, and neoclassical healing for a range of magnetic configurations.

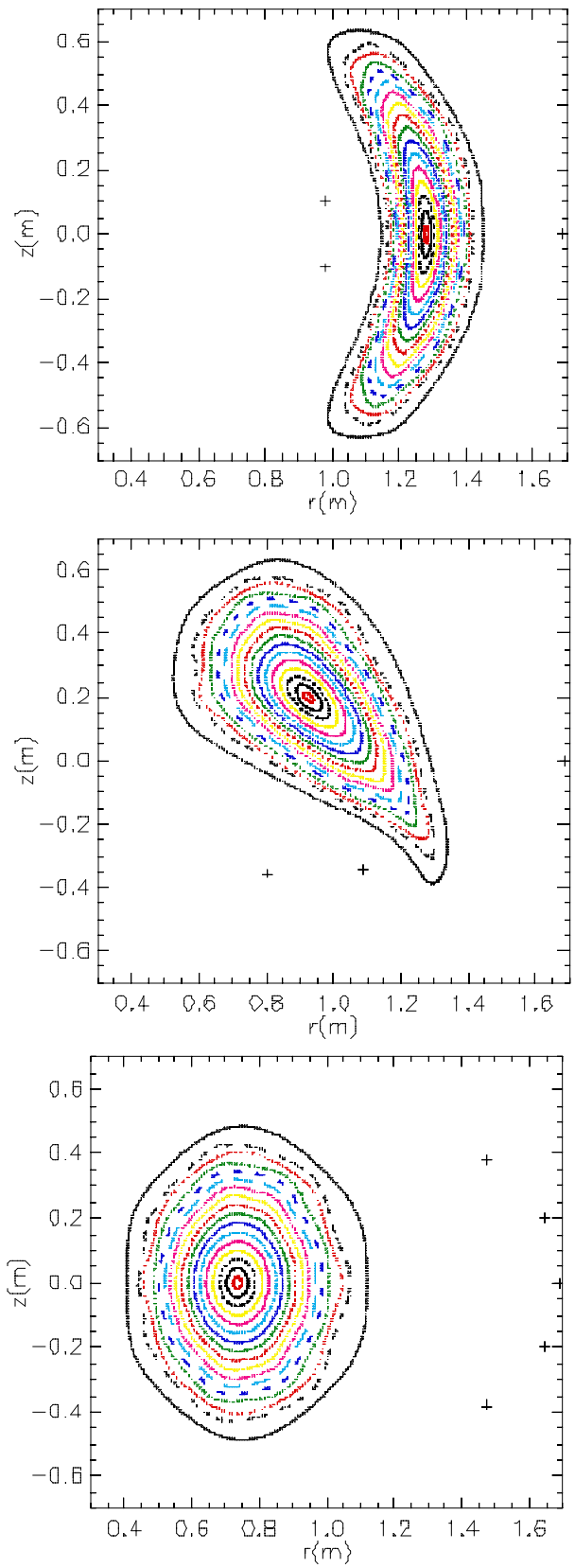

Figure 5.1. Vacuum flux surfaces from AVAC for the reference configuration.

5.3. Calculation of Finite Pressure QPS Equilibria

5.3.1. VMEC Equilibria

The 3D equilibrium code VMEC [2] obtains equilibria by minimizing the plasma potential energy $\int (B^2/2 + p)dV$. The VMEC code assumes nested flux surfaces exists and therefore does not allow for the existence of magnetic islands. We expect that the VMEC solutions are good approximations of real equilibria when magnetic islands are small. Details of this equilibrium code are contained in Appendix A.

The VMEC equilibrium is sensitive to the current in the external coils. A portion of the outer flux surface with a cross section of the inner surfaces for a free-boundary calculation of the reference configuration at <β> = 2% are shown in Fig. 5.2. Flux surfaces for this configuration are shown in Fig. 5.3. This calculation was performed using the modular coil set described in Chapter 4.

For comparison, Fig. 5.4 shows the cross sections for the fixed boundary equilibrium used to design the coils. A direct comparison of the outer cross sections of the fixed and free boundary VMEC calculations for the reference configuration is shown in Fig. 5.5 (same as Fig. 4.7). The outer surfaces are very similar for the two calculations. The χ^2 errors (weighted mismatch between targeted and actual physics parameters) for selected optimization parameters for the free and fixed boundary calculations are shown in Table 5.1. Comparing the ratios of χ^2 for the two calculations indicates the coils are able to reproduce the physics properties of the fixed boundary configuration. Note that the reference coil configuration was generated using an unoptimized pressure profile that was slightly ballooning unstable at several surfaces. This gives rise to the nonzero ballooning χ^2 in the table. With optimized pressure profiles (see below), both of free and fixed boundary configurations are ballooning stable at beta = 2% and have an associated $\chi^2 = 0$.

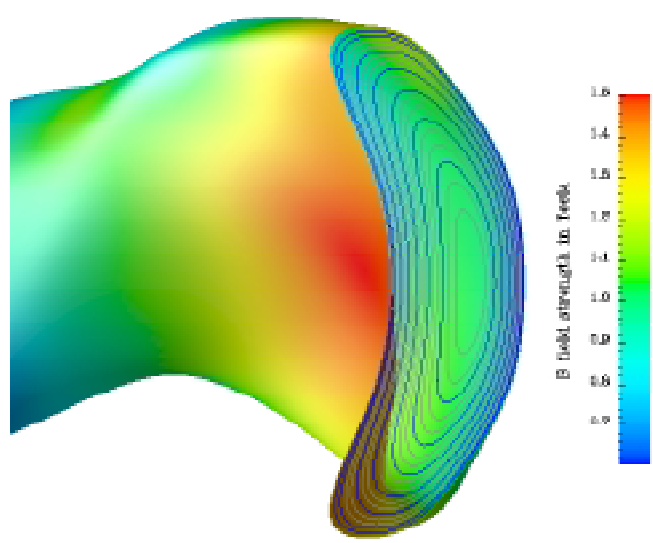

Figure 5.2. Partial outer surface and cross sections of the reference configurations.

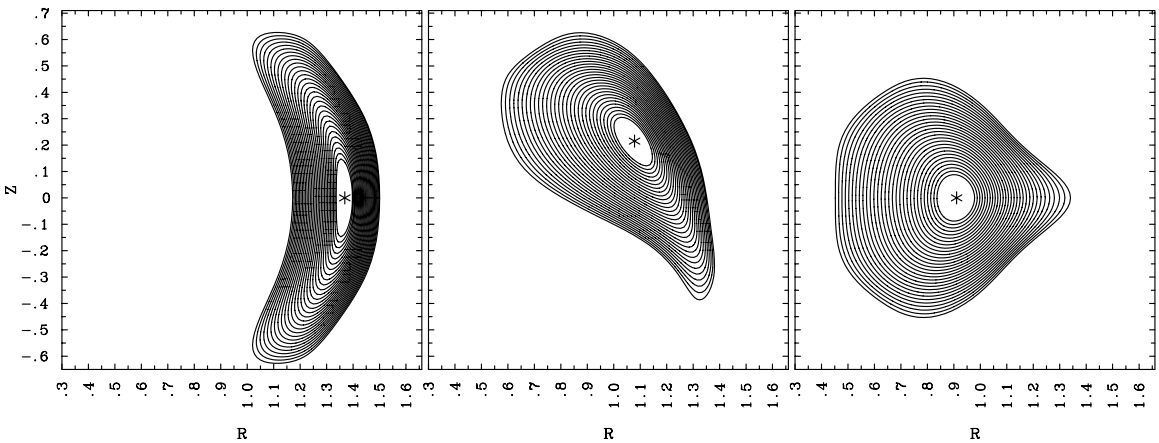

Figure 5.3. Free-boundary cross sections of the flux surfaces at <β> = 1.9% for the reference coil configuration with I_{mod} = 374 kA, I_{VF} = –205 kA, and I_{TF} = –341 kA.

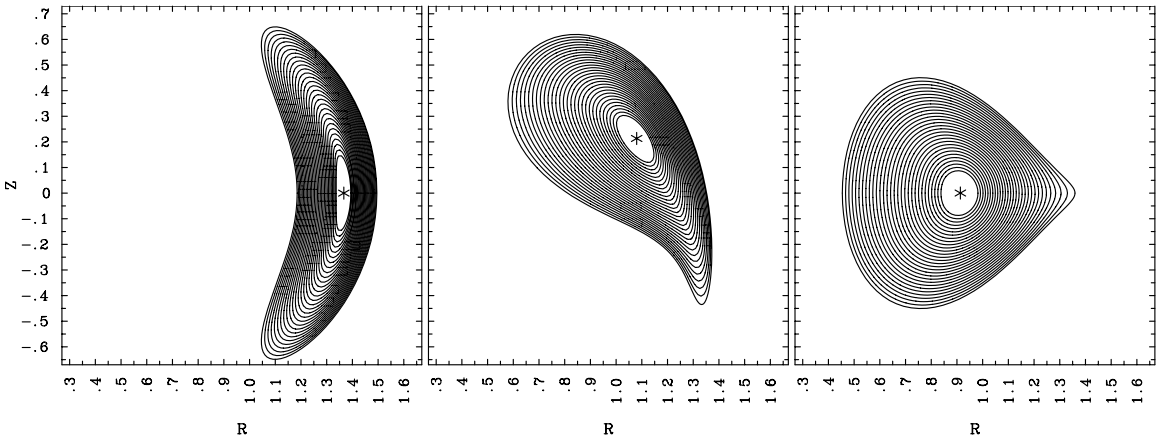

Figure 5.4. Fixed-boundary cross sections of the reference configuration.

Table 5.1. χ^2 values for selected optimization parameters for the free and fixed boundary calculations

	χ^2 (Balloon)	χ^2 (DKES)	χ^2 (Bootstrap)
Fixed Boundary	1.9×10^5	6.2×10^4	1.3×10^5
Free Boundary	3.6×10^5	6.0×10^4	6.6×10^4

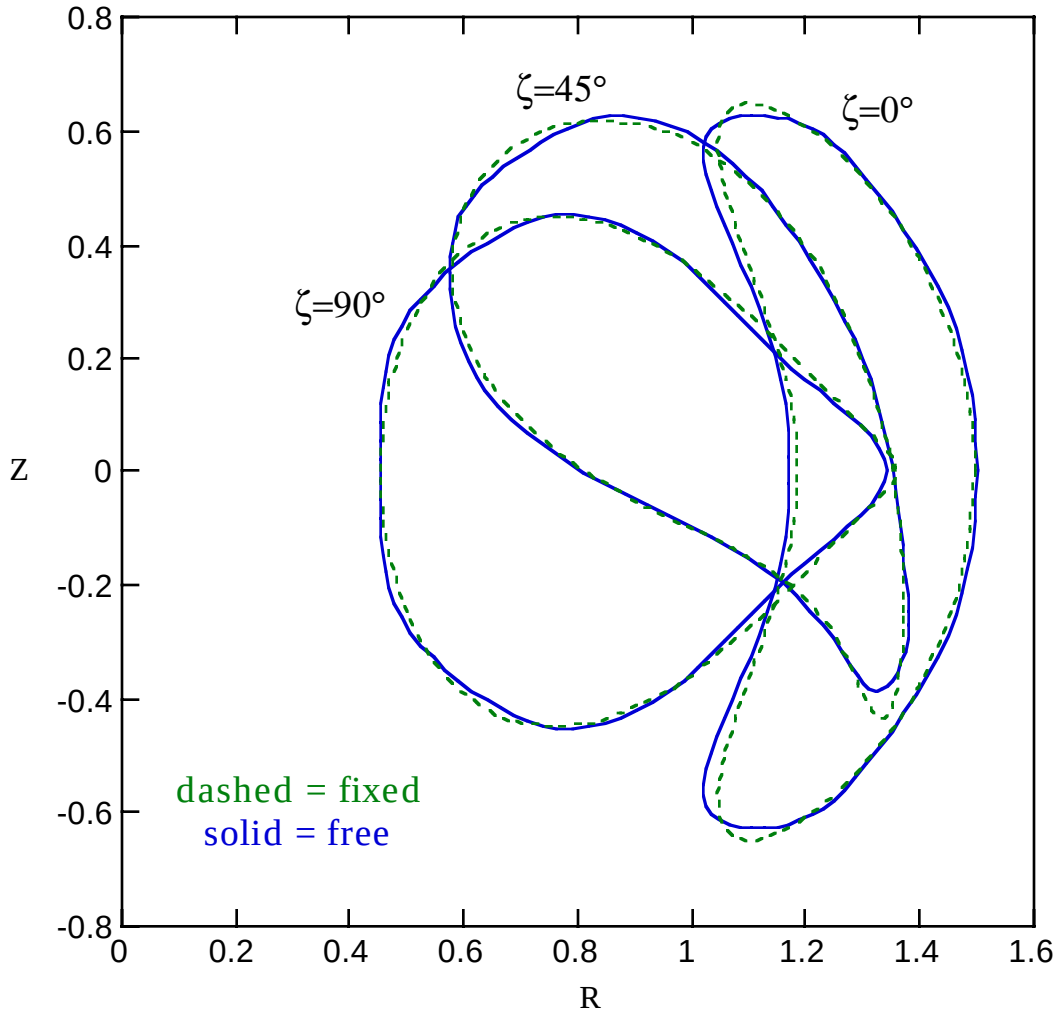

Figure 5.5. Outer cross sections for free and fixed boundary calculations of the reference case.

5.3.2. PIES Equilibria

The PIES [3,4] code is a three-dimensional equilibrium code that uses a general representation for the field, and is therefore capable of calculating islands and stochastic field line trajectories. Details of the PIES code are discussed in Appendix A. The PIES code is used to test for the existence of magnetic islands in the QPS reference configuration and to verify the existence of good surfaces at finite β.

Figure 5.6 compares Poincaré plots at the half-period toroidal symmetry plane (v = 1/2) obtained from fixed-boundary PIES calculations for the reference ⟨β⟩ = 2% QPS configuration. The top half of the figure shows a set of small magnetic island chains and the bottom half shows the result of varying the boundary modes (m,n) = (1,6), (1,5), (1,4), (1,3), (1,2), (2,6), (2,5), (2,4), (2,3), (2,2), (3,6), and (3,5) and targeting the (1,6), (2,12) and (2,11) resonances. The initial set of islands for the reference configuration are reduced,

although they were not large before the surface healing process. Larger magnetic islands, as occurred in the initial NCSX configurations, could also be removed by a small adjustment of the boundary shape in NCSX that had little impact on the other physics properties. In regions where $d\iota/ds > 0$, the positive bootstrap current is predicted to lead to decreased magnetic island widths in configurations of the type studied here. This is related to the neoclassical stabilization of tearing modes that has been observed in tokamak experiments. This neoclassical effect is being incorporated in the PIES code, but has not been included in any of the calculations reported here. The calculations are therefore conservative in that the calculated island widths are likely to be larger than would be observed in an experiment operated in a collisionless regime.

Calculations of free-boundary PIES equilibria were successful for the NCSX magnetic configuration, but the PIES code has difficulty in calculating QPS equilibria because of the sharp corners in the low-aspect-ratio equilibrium flux surfaces. These points in the surface are near a separatrix and PIES has a difficulty in extrapolating these surface to create a vacuum region outside the last closed VMEC surface. A singularity tends to develop in these vacuum surfaces outside the plasma. Techniques to address this issue need to be further explored.

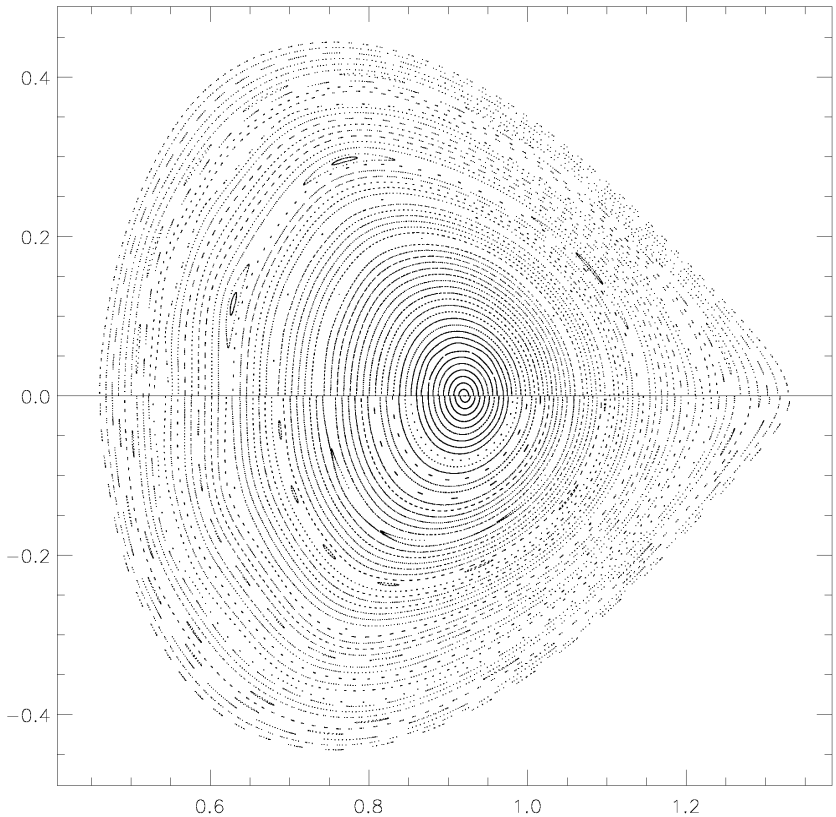

Figure 5.6. Poincaré plots from fixed-boundary PIES calculations of the reference QPS configuration before (top half) and after (bottom half) the NCSX island healing process.

A variation of the reference QPS coil configuration with unequal currents in the modular currents was successfully analyzed for flux surface quality with the PIES code. This $\langle\beta\rangle$ = 2% QPS case had slightly smaller field errors (δB_{avg} = 1.1%, δB_{max} = 6.0%) but less favorable coil-coil separation ($\Delta_{cc,min}$ = 10.5 cm) and minimum radius of curvature (ρ_{min} = 4.6 cm). Figure 5.7 shows a fixed-boundary Poincaré plot for this coil set in a polar (ρ, θ) coordinate system which makes the magnetic field structure more readily visible. In this plot the vertical coordinate ρ is constant on VMEC flux surfaces, and the distance of the VMEC flux surface from the magnetic axis is measured along the $\theta = 0$, $\phi = 0$ line. The horizontal (angular) coordinate θ is identical to the VMEC angular coordinate. When plotted in these coordinates, the Poincaré plot gives straight lines when the VMEC and PIES solutions coincide. The closed surface at small ρ is due to the difference in VMEC and PIES coordinates.

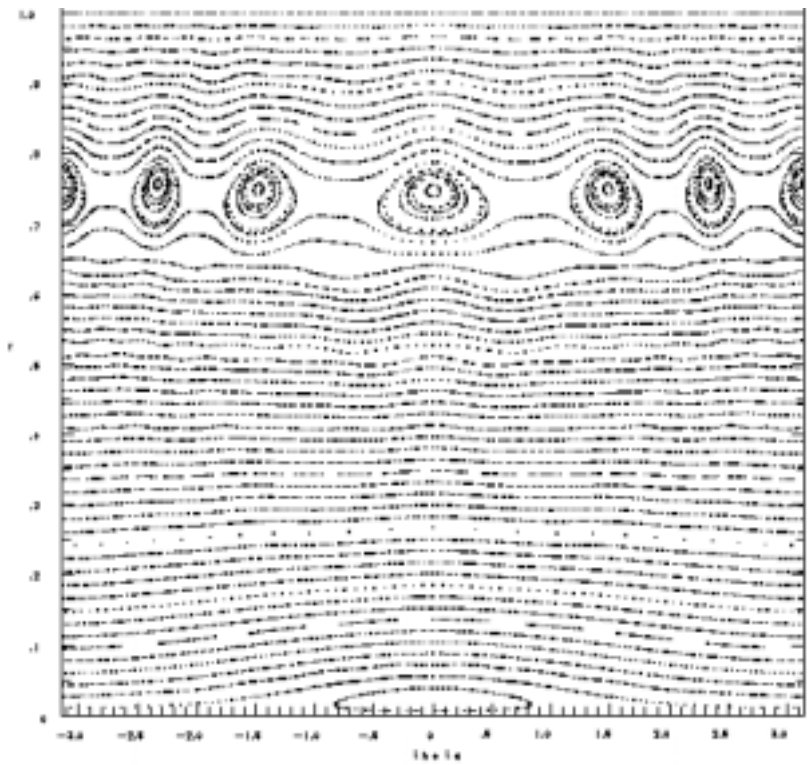

Figure 5.7. Fixed-boundary PIES Poincaré plot for a QPS configuration with unequal currents in the modular coils.

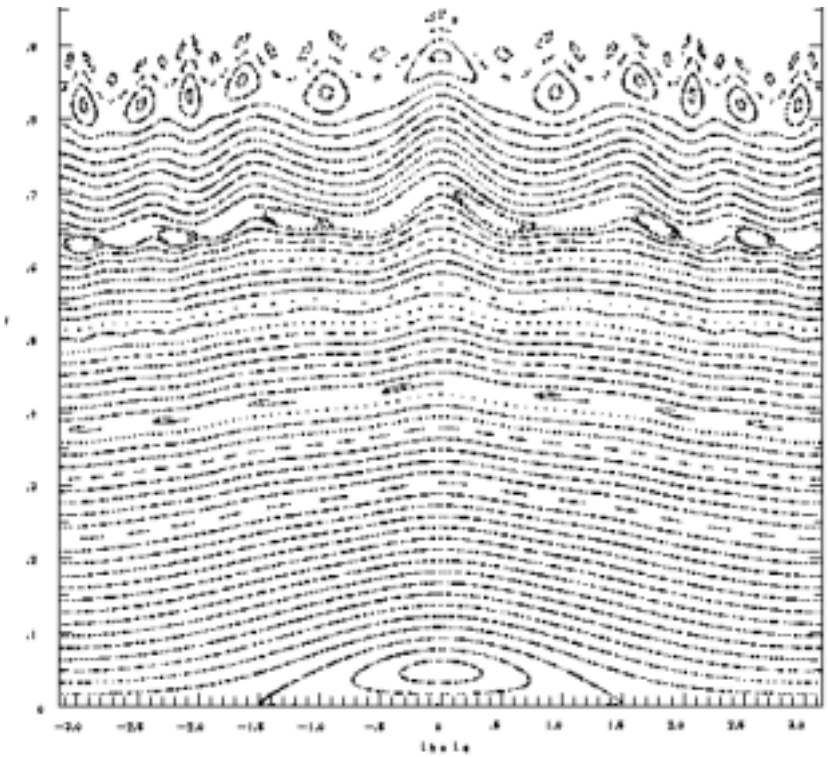

Figure 5.8. Free-boundary PIES Poincaré plot for the case shown in Figure 5.6.

A chain of m = 6, n = 2 islands is seen in Figure 5.7 around ρ = 0.75 where a low-order rational surface (ι = 1/3) would exist. The size of the islands is larger in this case than for the reference configuration in Figure 5.6. The free-boundary PIES calculation corresponding to this case is shown in Figure 5.8 in ρ-θ coordinates and in Figures 5.8 and 5.9 in normal z-R coordinates. The bounding surface in Figures 5.9 and 5.10 is a computational boundary that is 5% larger than the LCFS for the fixed-boundary equilibrium to allow surfaces to protrude into the vacuum region outside the fixed-boundary LCFS. At this stage in the calculation, the 2/6 island chain (around ρ = 0.65) has diminished in size, but a 4/11 island chain has appeared that is disrupting the surface. The calculation in Figures 5.8-5.10 has not fully converged. Extending this calculation further leads to deterioration of the flux surfaces. An earlier reference case started with an island chain as large as that shown in Figure 5.7 and converged to an equilibrium similar to that shown in Figure 5.8.

This case and the initially smaller island size for the QPS reference case support optimism that the reference case will also converge to a reasonable equilibrium state, but this has not been demonstrated and it may take further effort due to the difficulty in treating this case with PIES.

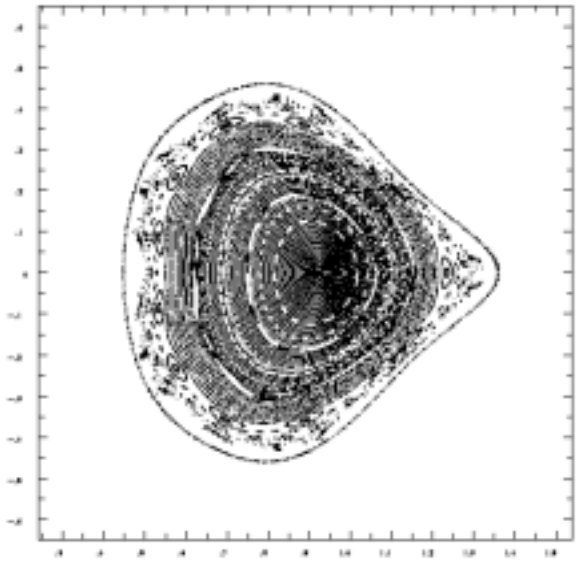

Figure 5.9. Free-boundary PIES Poincaré plot in normal space coordinates for the case shown in Figure 5.7.

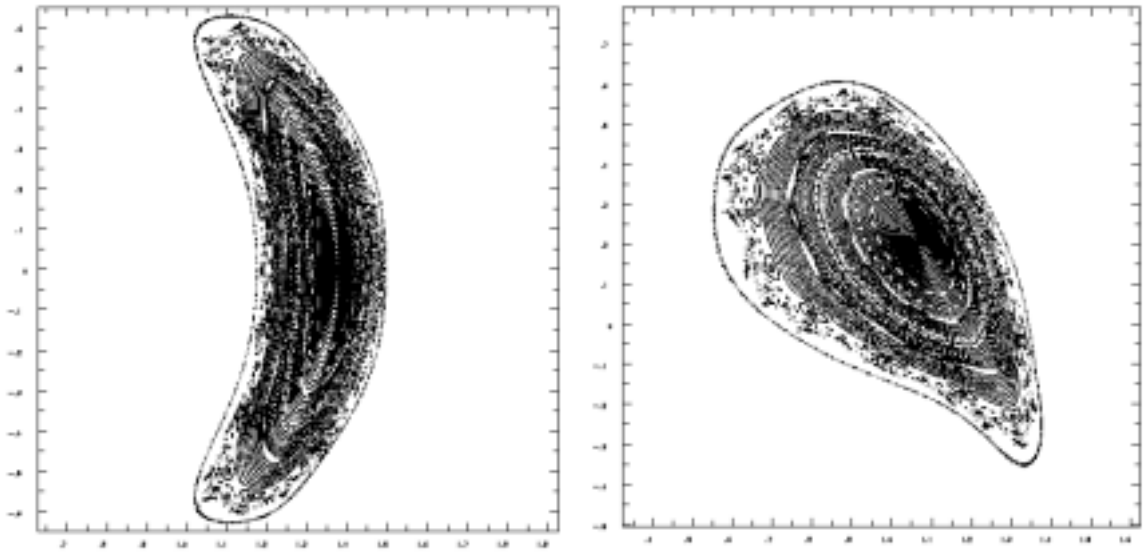

Figure 5.10. Free-boundary PIES Poincaré plots in normal space coordinates for the case shown in Figure 5.8 at v = 0 (left) and v = 1/4 (right).

5.4. Bootstrap Current Consistency

5.4.1. Bootstrap alignment of the reference configuration.

The current profiles in the reference configuration for the QPS experiment have been designed for alignment with the bootstrap current calculated from the VMEC equilibria. This means that the bootstrap current, which is calculated numerically based on a low-collisionality formulation [5], should approximate the surface-averaged parallel current

required for equilibrium. (The bootstrap current is therefore *consistent* with the magnetic spectrum of the configuration.) The VMEC equilibrium current and the predicted bootstrap current profiles for the reference configuration are shown in Fig. 5.11 for β =2%. The degree of agreement between the equilibrium and bootstrap currents is quite good. Also shown in Fig. 5.11 is the predicted bootstrap current for an equivalent tokamak which is a factor of 2-3 larger than the bootstrap current in the QPS configuration.

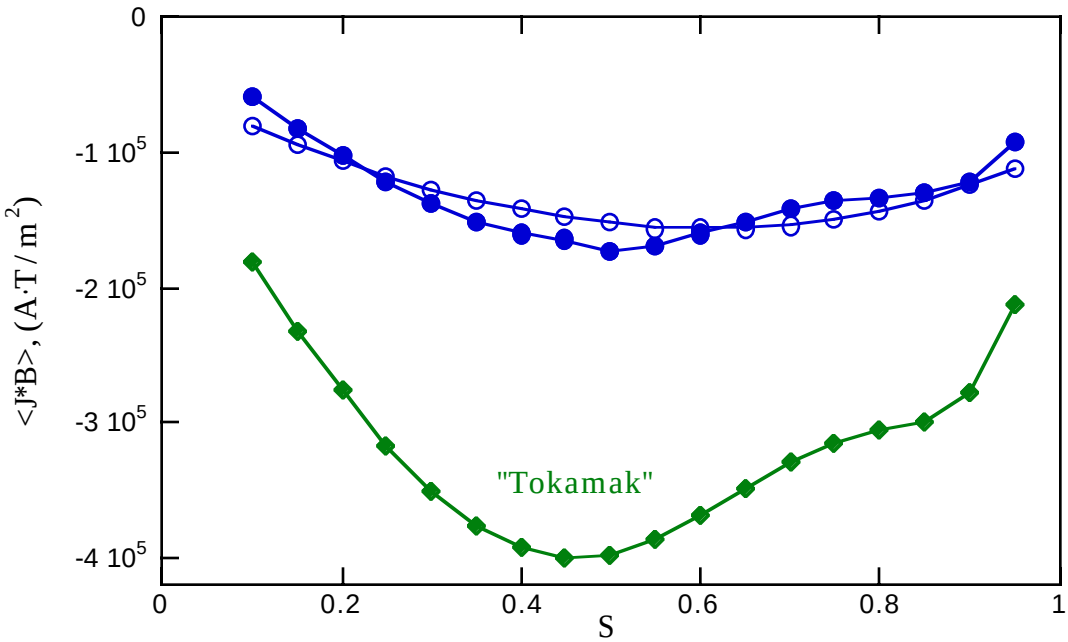

Figure 5.11. Field-aligned current profiles from a fixed boundary VMEC equilibrium (open circles), predicted bootstrap (closed circles), and the bootstrap current in an equivalent tokamak (green).

5.5. Neoclassical Healing of Magnetic Islands

The direction of the bootstrap current in the QPS configuration is such that it adds to the existing external rotational transform arising from coils. Because the relationship j_{BS} d ln $|\iota|/d\phi > 0$ is satisfied, the effect of bootstrap current should be to reduce (heal) magnetic island widths [6] for finite-β QPS equilibria. Presently, the PIES code is unable to simulate this effect. Part of the QPS experimental program will be to investigate neoclassical healing (or its reverse, island enhancement) by altering the sign of the rotational transform through changes in the external coil currents.

5.6. MHD Stability Properties

All the stability codes used here use equilibrium input from the VMEC code and are therefore based on the assumption that nested (good) magnetic surfaces exist, at least locally. For a more detailed description of the codes, see Appendix A.

5.6.1. Description of MHD Stability Codes

The VMEC equilibrium code evaluates the Mercier stability criterion based on the formulation of Ref [7].

The Code for Ballooning Rapid Analysis (COBRA) [8] was developed as part of the NCSX/QPS design project to provide an efficient analysis of ballooning stability for compact, highly shaped stellarator configurations. The desire to include this analysis inside a stellarator optimization code was a primary motivation for its development, since previous ballooning stability calculations were sufficiently slow to require post-optimization analysis. Significant speed enhancements (factors of hundreds of times) relative to previous codes [9] have been achieved. Recently, a VMEC coordinate-based version of COBRA [10] has been developed as a result of several convergence problems associated with conversion into Boozer flux coordinates. Namely, the marginal stability properties were sometimes sensitive to the number of Boozer Fourier modes used in the transformation from VMEC coordinates.

The three dimensional ideal MHD stability code TERPSICHORE [9] is used to calculate the stability of global (low n) MHD modes. The code determines the eigenvalues of the ideal MHD equations by minimizing the perturbed plasma potential energy. It has been used to analyze the stability of QPS configurations to both vertical (n=0) and kink (n=1) modes. More details of the TERPSICHORE code can be found in Appendix A.

5.6.2. Mercier stability of reference configuration.

The QPS reference configuration is stable over the entire plasma cross-section except for a few isolated resonances (Fig. 5.12). This configuration has a substantial well over the entire plasma cross section due to a combination of helical curvature and a small Shafranov shift (see Fig. 5.13). .It is stabilized primarily by the well rather than the shear (bending) terms in the Mercier criterion (Figure 5.14). This applies everywhere except near the edge, where the destabilizing geodesic curvature is small anyway. The terms arising from the net parallel bootstrap current are stabilizing but small. The strong well stabilization implies that high-n resistive modes should also be stable in this configuration.

The reference configuration was optimized for Mercier and ballooning stability at $<\beta>=2\%$. A sequence of plasmas at $<\beta>$ = 2, 3, 4, and 5% with toroidal plasma current scaled as 59, 83, 101, and 112 kA, respectively, were obtained in order to test the stability of the QPS configuration at higher β. As β increases, the magnetic well deepens (Fig. 5.15). At β = 3%, the plasma remains Mercier stable across the entire cross section. At β = 4% and 5%, 1/5 of the outer cross section becomes first weakly and then strongly Mercier unstable.

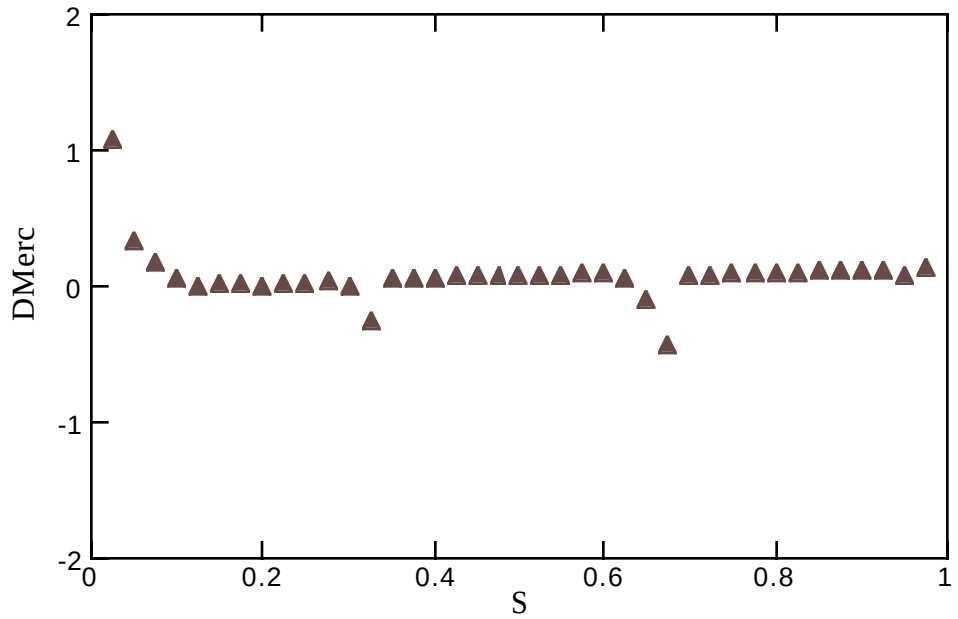

Figure 5.12. Mercier stability criteria for the free-boundary reference configuration.

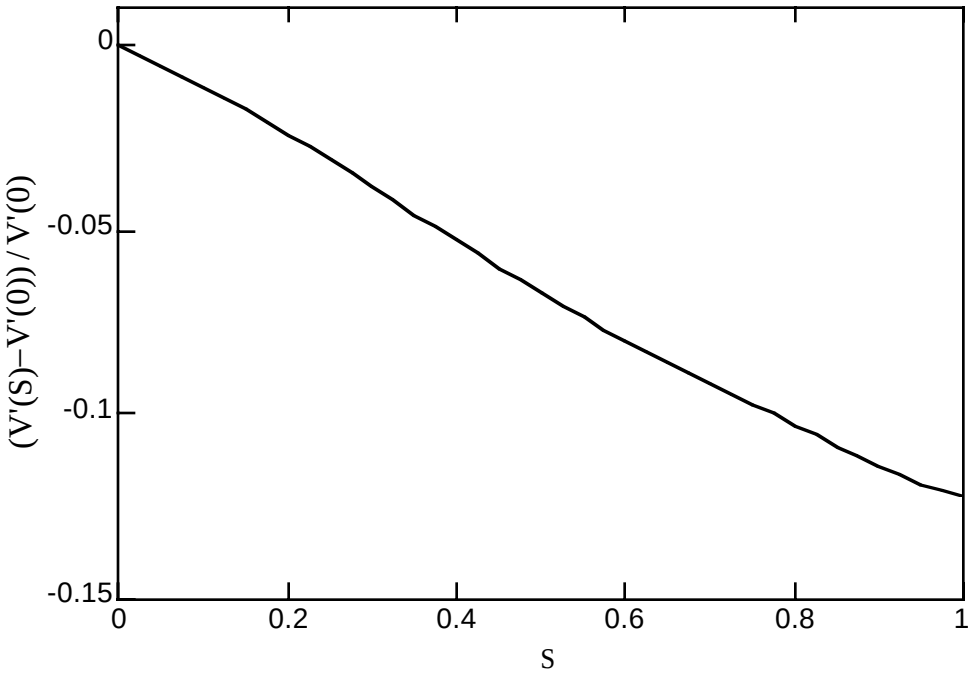

Figure 5.13. The magnetic well for the reference configuration at <β> = 2%.

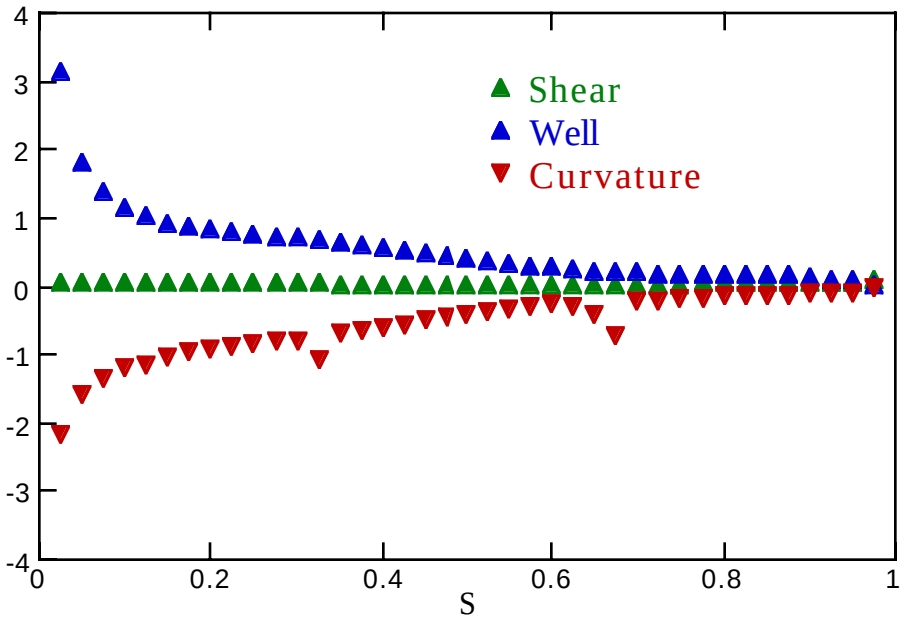

Figure 5.14. Components of the Mercier stability criteria for the reference configuration.

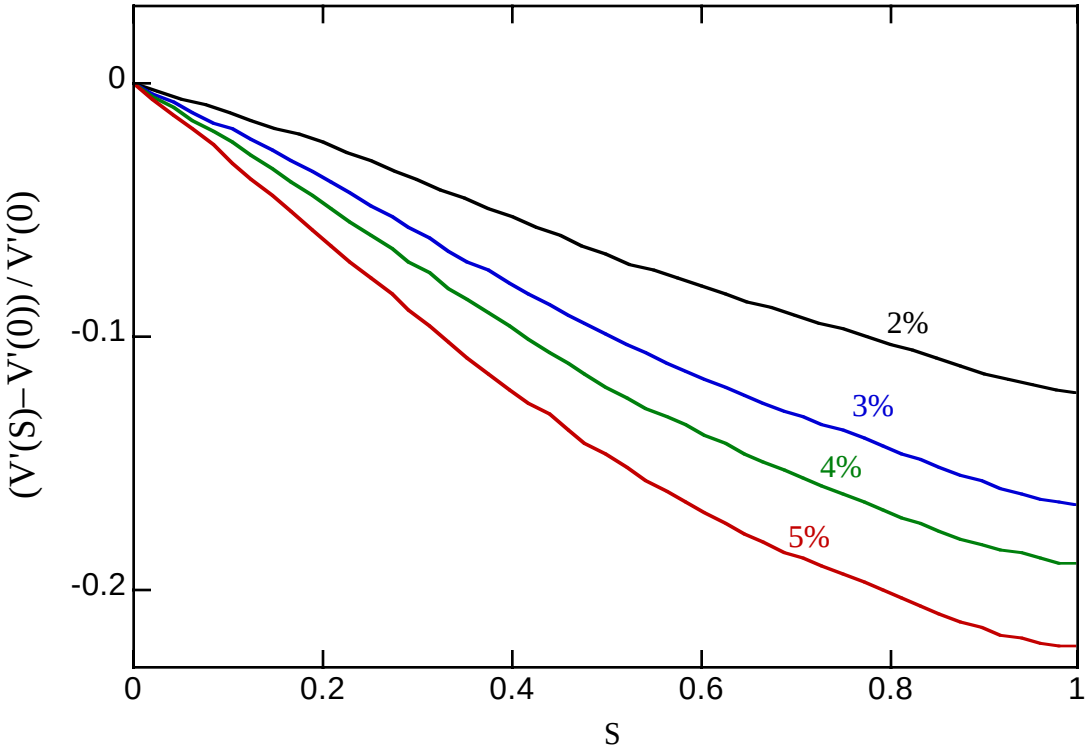

Figure 5.15. The magnetic well for the reference configuration at <β> = 2%.

5.6.3. Ballooning stability of reference configuration.

The QPS reference configuration is sensitive to ballooning modes as analyzed by the COBRA code. These set the β MHD stability limits for the reference configuration. The field line-bending term is weakened as a result of the small number of field periods (the connection length R/N is relatively long). This seems to be the dominant adverse effect on stability in QPS.

The pressure profile for the reference configuration has been optimized for ballooning stability at $<\beta>=2\%$, with the constraint $dp/d\phi = 0$ at the plasma edge to avoid edge currents. The optimized pressure profile is shown in Fig. 5.16. The ballooning growth rate (positive is unstable) of the reference configuration is shown in Fig. 5.17. As β is increased above 2% (by scaling the pressure profile and increasing the plasma current to maintain bootstrap alignment), a region of instability appears in the outer half of the plasma for $<\beta> > 2.2\%$ (Fig. 5.18). For a coil configuration similar to the reference case, free boundary equilibria with higher β limits were obtained by allowing an edge pressure pedestal. Those configurations had a β limit of > 2.5%. This class of profiles may develop naturally as a result of H-mode physics.

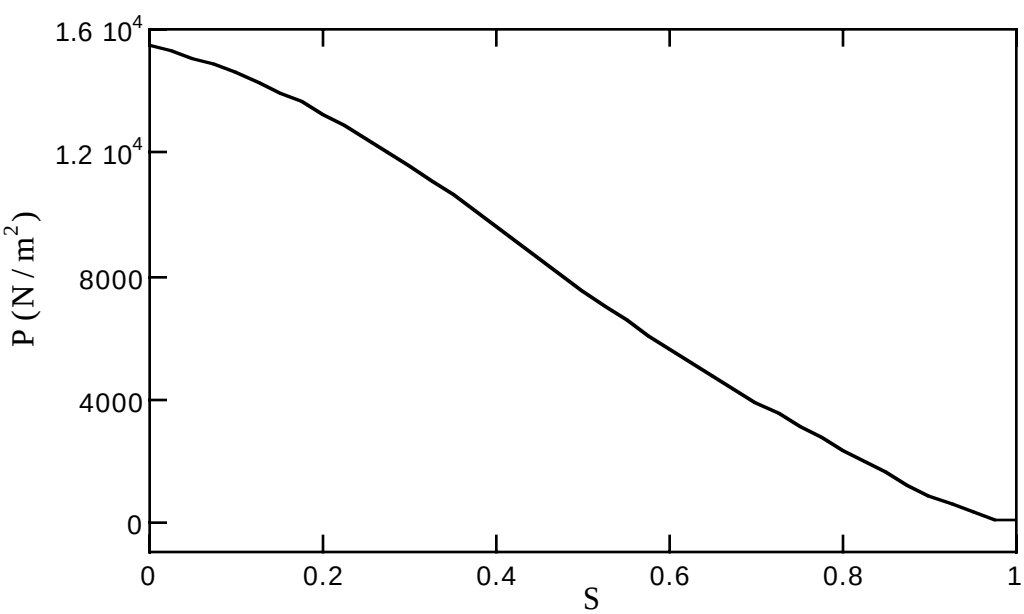

Figure 5.16. Optimized pressure profile for the reference configuration.

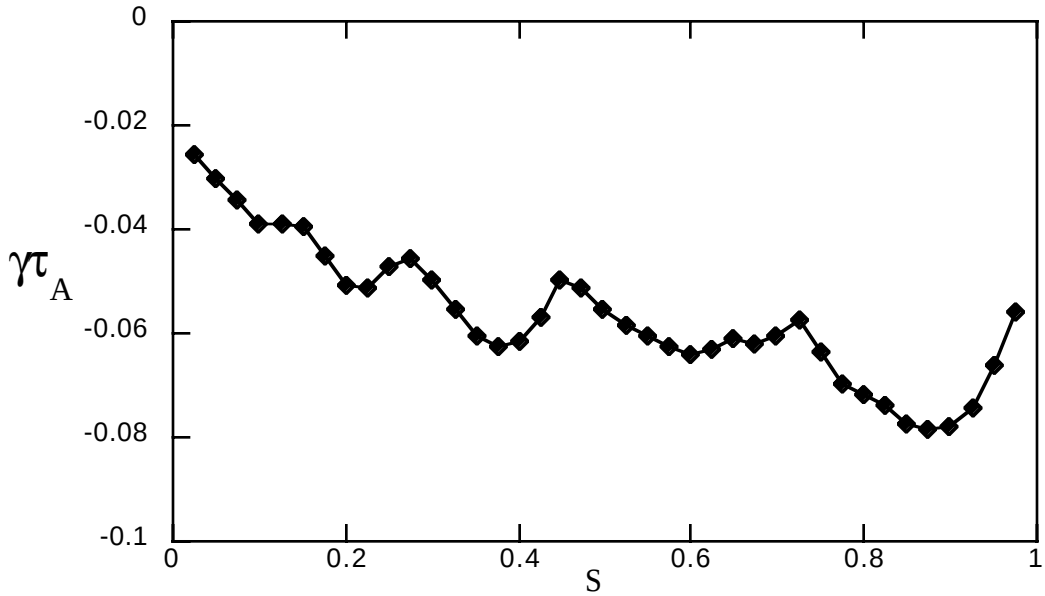

Figure 5.17. Ballooning growth rate normalized to the Alfvén time from COBRA for the reference configuration with the pressure profile shown in Fig. 5.16.

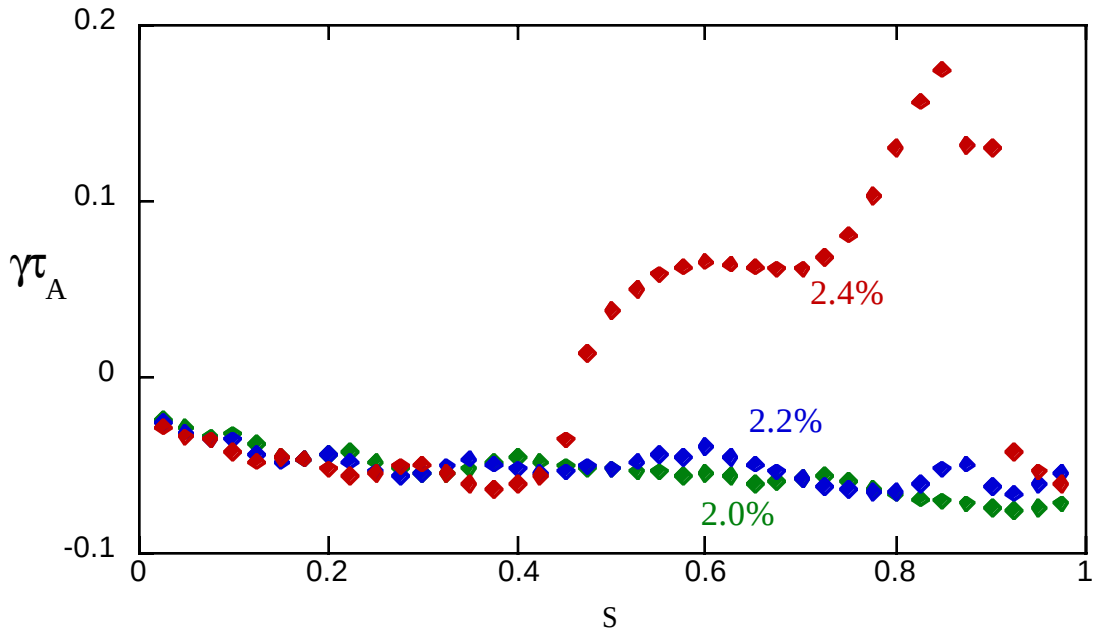

Figure 5.18. Ballooning growth rates for free boundary VMEC equilibria at <β> = 2.0, 2.2, and 2.4%.

5.6.4. External kink and vertical stability of reference configuration.

The finite current in the QPS configuration makes it necessary to address the issue of low-*n* ideal MHD modes which can be destabilized by current and pressure gradients. The TERPSICHORE stability code was used to analyze vertical (n=0) and kink (n=1) mode

stability of the reference configuration. This configuration is stable to both vertical and kink modes at <β>=2%. The vertical and kink stability of the previously mentioned free boundary beta scan up to <β>=5% were also analyzed. All the cases were stable to vertical modes. Only the <β>=5% case with toroidal current of 112 kA was unstable to kink modes with a kink eigenvalue of 5.4×10^{-4}.

The vertical stability is due primarily to the external rotational transform. An analytic stability criterion for vertical mode in a large aspect ratio current-carrying stellarator has been developed (for constant current density and constant external rotational transform) [11]. The stability criteria relates the fraction of edge rotational transform, $F \equiv \iota_{\text{external}} / \iota_{\text{total}}$, to the axisymmetric elongation, κ:

$$F \geq \frac{\kappa^2 - \kappa}{\kappa^2 + 1} \tag{1}$$

The external transform is stabilizing because the external poloidal flux enhances the field line bending energy relative to the current-driven term for the vertical instability. For the reference configuration, we have $F = 0.697$, $\kappa = 2.765$, and $\left(\kappa^2 - \kappa\right)/\left(\kappa^2 + 1\right) = 0.565$, resulting in the condition being well-satisfied. This criterion is met for all of the cases in the beta scan and is consistent with stability to vertical modes for all of these.

5.7. Resistive Stability and Tearing Mode Comments

The reference QPS configuration avoids the ι=0.5 surface everywhere in the plasma and has a monotonically increasing transform profile. In addition, the predicted bootstrap current is only a fraction of the typical Ohmic current in the equivalent tokamak. In addition, QPS configurations have a deep magnetic well which has a stabilizing influence on resistive modes. For these reasons, the resistive stability of QPS has not been considered to be an important issue. Moreover, the lack of any numerical codes for calculating resistive (tearing) modes in three-dimensional geometries compounds the difficulty of making an accurate prediction for the stability of such modes.

5.8. Conclusions

The reference coil configuration reproduces the physics of the fixed boundary VMEC equilibria. The vacuum and finite pressure surfaces are robust and are not overly susceptible to islands or ergodic regions.

The MHD stability limits are set by ballooning modes rather than kink or vertical modes. The ballooning beta limit is approximately 2.2%. The actual ballooning beta limit may be higher than this limit if pressure profiles with edge pedestals are obtained. Kink and vertical modes are not an issue for the QPS configuration.

References

[1] D. K. Lee, Comput. *Phys. Comm*. 25, 181 (1982).

[2] S. P. Hirshman and J. C. Whitson, *Phys. Fluids* **26** 3553 (1983).

[3] A. Reiman and H. S. Greenside, *Comput. Phys. Commun*. **43** (1986) 157.

[4] A. Reiman and H. S. Greenside, *J. Comput. Phys*. **75** (1988) 423.

[5] K. C. Shaing,, E.C. Crume, Jr., J.S. Tolliver, S.P. Hirshman, W.I. van Rij, Phys. Fluids B1, 148 (1989).

[6] C. C. Hegna and J. D. Callen, *Phys. Plasmas* **1** (1994) 3135.

[7] F. Bauer, O. Betancourt, P. Garabedian,: "*Magnetohydrodynamic Equilibrium and Stability of Stellarators"*, Springer-Verlag, New York, 1984).

[8] R. Sanchez, S. P. Hirshman, J. C. Whitson, and A. S. Ware, *J. Comput. Physics* **161**, 576 (2000).

[9] D. V. Anderson, W. A. Cooper, R. Gruber, S. Merazzi, and U. Schwenn, Scient. Comp. Supercomputer II, 159 (1990).

[10] R.Sanchez, et. al., submitted for publication to C*omput. Physics Comm*. (2001).

[11] G. Y. Fu, *Phys. Plasmas* **7**, 1079 (2000).